JACS
JOURNAL OF THE AMERICAN CHEMICAL SOCIETY
Article
pubs.acs.org/JACS

Determination of Redox Reaction Rates and Orders by In Situ Liquid Cell Electron Microscopy of Pd and Au Solution Growth

Eli A. Sutter* and Peter W. Sutter

Center for Functional Nanomaterials, Brookhaven National Laboratory, Upton, New York 11973, United States

Supporting Information

ABSTRACT: In-situ liquid cell transmission and scanning transmission electron microscopy (TEM/STEM) experiments are important, as they provide direct insight into processes in liquids, such as solution growth of nanoparticles, among others. In liquid cell TEM/STEM redox reaction experiments, the hydrated electrons e^-_{aq} created by the electron beam are responsible for the reduction of metal-ion complexes. Here we investigate the rate equation of redox reactions involving reduction by e^-_{aq} generated by the electron beam during in situ liquid TEM/STEM. Specifically we consider the growth of Pd on Au seeds in aqueous solutions containing Pd-chloro complexes. From the quantification of the rate of Pd deposition at different electron beam currents and as a function of distance from a stationary, nanometer-sized exciting beam, we determine that the reaction is first order with respect to the concentration of hydrated electrons, $[e^-_{aq}]$. By comparing Pd- and Au-deposition, we further demonstrate that measurements of the local deposition rate on nanoparticles in the solution via real-time imaging can be used to measure not only $[e^-_{aq}]$ but also the rate of reduction of a metal-ion complex to zerovalent metal atoms in solution.

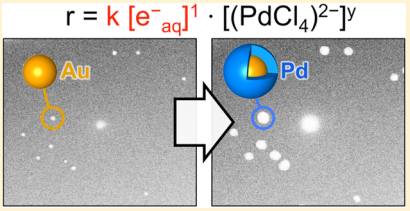

1. INTRODUCTION

There has been a lot of interest in in situ transmission electron microscopy (TEM/STEM) approaches, which allow following in real time processes in wet environments that span colloidal synthesis of nanoparticles,[1−3] rods,[4] and core−shell nanostructures,[5] galvanic replacement reactions,[6] assembly of nanoparticles,[7] electrochemical deposition,[8] stability of liquid fuel cell electrolytes,[9] biological systems,[10,11] etc. High-resolution TEM/STEM imaging of processes in liquids was made possible by the development of microfabricated liquid cells consisting of two electron transparent membranes between which a small volume of liquid is confined. Liquid TEM/STEM is a powerful technique in which a collimated or focused beam of high-energy electrons enables imaging in liquids with subnanometer resolution, but the beam also invariably affects the systems under investigation due to the interaction of the imaging electrons with the liquid confined in the cell, as well as with objects dissolved or suspended in the liquid.

The beam interactions can have different consequences. Imaging of biological systems such as cells,[10] proteins,[12] or macromolecular complexes[13] has been demonstrated in their native environment (i.e., water), but such experiments are complicated by radiation damage due to the electron beam. Enzymatic deactivation occurs within the first image frame,[14] but structural damage may take longer to manifest itself, thus permitting structural observations in aqueous environments. When imaging nanoparticles in solution, the electron beam can alter the motion of nanoparticles. On one hand, this prevents following the unperturbed behavior of suspended particles,[15,16] but on the other hand, beam effects can also be used purposely, e.g., to induce the movement of nanodroplets on the membrane of the cell.[17,18] Another example of a beneficial "disturbance" is the ability of the electron beam to reduce metal-ion complexes in solution, which has enabled the investigation of nucleation, growth, and movement of nanoparticles,[1,2,19] nanowires,[20] and core−shell nanostructures[5] without the need of providing additional reducing agents or applying external bias. The recognition that radiolysis by the high-energy electron beam produces radicals that can induce or modify chemical reactions in solution has triggered work on understanding the effects of the electron beam[3,6,21] and determining the distribution of radiolysis products, e.g., hydrated electrons responsible for the reduction of metal-ion complexes in aqueous solution.[5]

Formally, hydrated electrons (e^-_{aq}) can be considered as a reactant in redox reactions that lead, for instance, to the deposition of Pd from Pd-chloro complexes (such as tetrachloropalladate $[(PdCl_4)^{2-}]$ ions) following their reduction by the capture of 2 electrons: $(PdCl_4)^{2-} + 2e^- \rightleftharpoons Pd + 4Cl^-$.[5] By varying the reactant concentration, $[e^-_{aq}]$, it should be possible to determine the overall reaction order with respect to the hydrated electrons. The order of a reaction $A + B \rightleftharpoons C$ with respect to a reactant A is the exponent (x) to which its concentration, $[A]$, is raised in the rate equation $r = k[A]^x[B]^y$. Reaction orders need to be determined experimentally and are important, as their knowledge provides insight into reaction mechanisms and helps identify reaction-limiting steps, etc. While optical signatures can be used to track the concentration of hydrated electrons in aqueous solutions,[22] there is no direct way of measuring $[e^-_{aq}]$ generated by high-energy electrons in a TEM liquid cell. In the low-dose regime, however, their concentration is expected to be proportional to the electron

Received: August 20, 2014
Published: November 19, 2014

dx.doi.org/10.1021/ja508279v | J. Am. Chem. Soc. 2014, 136, 16865−16870

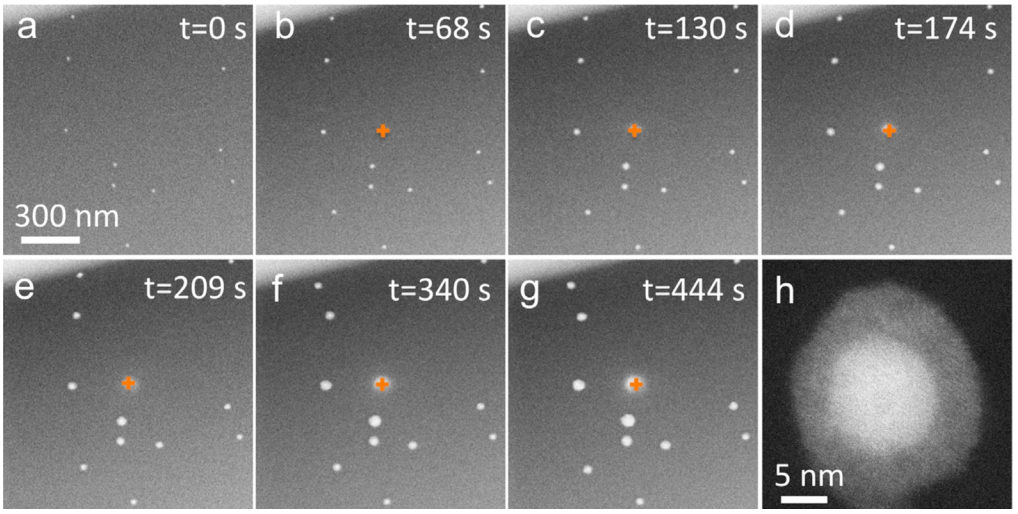

Figure 1. Electron beam induced growth of Pd on 12 nm Au seed nanoparticles in aqueous Pd salt solution. (a) Initial dark-field STEM image of an ensemble of 12 nm Au nanoparticles in 10 μM aqueous $PdCl_2$ solution. (a–g) Au growth, induced by cycles of local focused electron beam exposure (exposure time indicated in the individual frames; beam current: 200 pA; probe size: 0.2 nm) at the position marked by an orange cross. (h) Ex-situ HAADF STEM image of a Au–Pd core–shell particle formed in the initial growth regime. The bright feature at the position of the stationary beam spot (+) stems from local changes to the liquid cell membrane.

beam current for a given thickness of the liquid volume in the cell. Thus, changing the beam current represents one way of varying $[e^-_{aq}]$. A second approach involves the use of a local excitation by the electron beam, which generates a large concentration of hydrated electrons in a small, nanometer-sized area of the liquid cell. Diffusion of the long-lived e^-_{aq} sets up a well-defined gradient in the concentration $[e^-_{aq}]$ over a distance of nearly 1 μm from this source point. Similar to $[e^-_{aq}]$, the rate of reduction r of a metal-ion complex to a zerovalent metal can be measured indirectly by imaging the local deposition rate on seed nanoparticles in the solution, assuming a low supersaturation regime in which the particles represent perfect sinks for metal atoms; that is, no homogeneous nucleation of the metal species takes place in the solution.

Here we investigate the rate equation of redox reactions involving reduction by e^-_{aq} generated by the electron beam during in situ liquid TEM/STEM. Specifically, we consider the dependence of the growth of Pd and Au on Au seed nanoparticles suspended in dilute aqueous solutions of Pd- and Au-ion complexes. Using the rate of Pd (or Au) deposition at different electron beam currents and as a function of distance from a local injection site (i.e., excitation spot for radiolysis) as a measure of the rate of Pd^0 (Au^0) generation, we are able to determine the order of the redox reactions with respect to the concentration $[e^-_{aq}]$ of beam-generated hydrated electrons, the reducing agent in the in situ liquid cell electron microscopy experiments.

2. REACTION ORDER FOR REDUCTION OF Pd-ION COMPLEXES TO Pd^0 BY e^-_{aq}

Figure 1a shows an in situ liquid cell STEM image of the initial density and distribution of Au seed nanoparticles with diameter of ~12 nm in a 10 μM $PdCl_2$ solution. Figure 1b–g (and movies S1 and S2) follows the nanoparticles as their size increases due to the growth of Pd on their surface, initiated by the reduction of the Pd precursor by the electron beam.[5] In our experiments, the STEM probe (focused electron beam) with current of 200 pA was kept stationary for a given time duration at the center of the field of view, followed by imaging of a larger area surrounding this excitation spot by a single dark-field STEM scan at minimal additional electron dose. By repeating this excitation/imaging cycle, the progression of solution-phase reactions can be followed over extended time intervals and total electron doses. This approach essentially separates the two primary roles of the electron beam in liquid cell electron microscopy: (i) STEM imaging and (ii) the generation of reducing species, such as hydrated electrons and other anionic radicals produced by the beam. Radicals are formed primarily in a well-defined local excitation area, whereas their effect in driving redox reactions in solution is imaged under conditions that minimize the generation of additional radicals dispersed across the field of view.

The distribution and number of Au nanoparticles in the group in Figure 1 remain unchanged over time. Pd growth shows the overall characteristics of the growth on small Au seeds described earlier: Pd^0 deposition occurs preferentially on the Au nanoparticles, without any additional homogeneous nucleation and growth of Pd particles in the solution; the amount of Pd deposited on the Au seeds increases with time; and Au particles closer to the beam excitation spot experience faster Pd growth. The absence of homogeneous nucleation in the solution confirms a simple growth mechanism, in which the reduced Pd^0 is entirely captured by the Au seeds.[5] Pd is deposited uniformly over the surface of the particles, which results in the formation of epitaxial shells (Figure 1h). Consistent with previous results,[5] the growth rate of the Pd shells is not uniform across the field of view, but it is higher near the center where the electron beam is positioned and falls off toward the periphery away from the spot at which the electron beam is held stationary. Thus, the growth rate clearly depends on the distance from the excitation, in a way that is consistent with the high-energy electrons locally producing radicals, including hydrated electrons, which are distributed across the field of view by diffusion in the solution and give rise to a gradient in the concentration $[e^-_{aq}]$ away from the excitation spot.

dx.doi.org/10.1021/ja508279v | J. Am. Chem. Soc. 2014, 136, 16865–16870

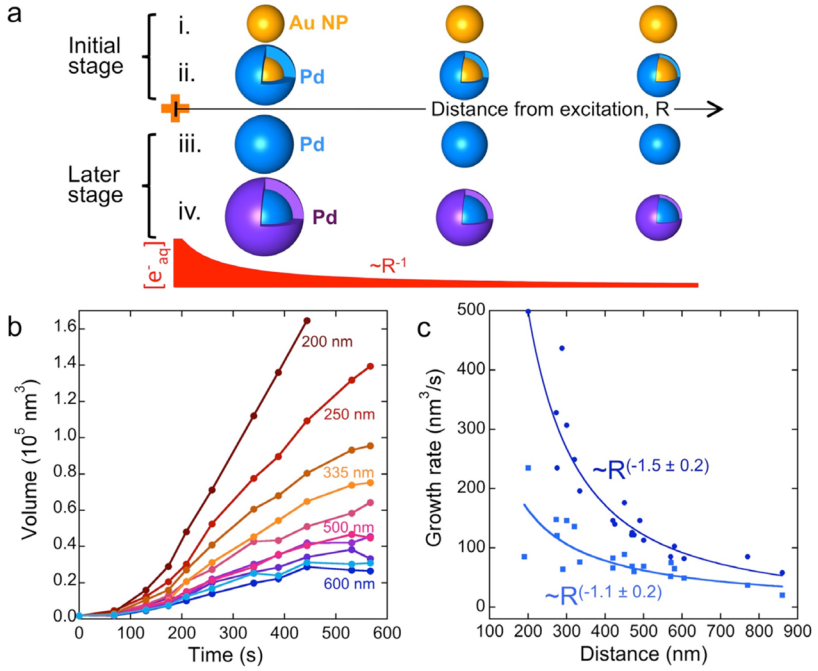

Figure 2. (a) Schematic showing growth of Pd on Au seed nanoparticles at two stages: i and ii. Initial stage: all nanoparticles have the same size and the volume growth rate depends only on the concentration of hydrated electrons, $[e^-_{aq}] \sim R^{-1}$ (bottom, red); iii and iv. Later stage: Particles closer to the excitation are now larger and the volume growth rate depends on both $[e^-_{aq}]$ and the particle surface area, *A*. (b) Experimentally determined dependence of the particle volume as a function of the time for particles (from Figure 1; movies S1 and S2) at different distances from the excitation spot (beam current: 200 pA). For clarity, only a subset of all analyzed growth curves are shown. (c) Dependence of the volume growth rate as a function of distance, determined for two different time regimes: initial growth rates for times between 0 and 180 s (light blue squares), and growth rates at a later stage ($t > 180$ s; dark blue circles). Solid lines are power law fits to the data. The analysis is based on a larger set of growth curves than are shown in b. (total of 20−25 data points for early- and later-stage growth, respectively).

Figure 2 shows an analysis of the time dependent volume increase due to Pd deposition on Au nanoparticles at different distances from the excitation spot. As shown in Figure 2a, we expect two distinct regimes for the time (t) dependence: (i and ii) initial growth starting with the bare Au nanoparticles, i.e., substrate particles that are all of the same size; (iii and iv) a later stage, in which different Pd growth rates as a function of distance from the exciting beam have produced significant variations in the size of the nanoparticles. The aqueous electrons, the primary species involved in reducing $(PdCl_4)^{2-}$ to Pd^0, are generated by radiolysis of water at the position of the stationary electron beam and diffuse outward. In steady state, the concentration profile, $[e^-_{aq}](R)$ is given by the diffusion equation,[5]

$$\frac{\partial[e^-_{aq}]}{\partial t} = D\nabla^2[e^-_{aq}] = D\frac{\partial}{\partial R}\left(R^2\frac{\partial[e^-_{aq}]}{\partial R}\right) = 0 \quad (1)$$

From the solution $[e^-_{aq}](R) = a/R + b$ (a and b are constants), we conclude that, with increasing distance R from the source, the concentration of aqueous electrons decreases as $[e^-_{aq}](R) \sim R^{-1}$ (Figure 2a). We assume that the growth of the Pd shell on Au nanoparticles is limited by the rate of the redox reaction in the solution, i.e., the rate at which e^-_{aq} reduces the $(PdCl_4)^{2-}$ precursor. The Pd growth rate scales with the generation rate of reduced Pd^0 (r) and the surface area (A) of the nanoparticles (i.e., the area capturing Pd^0):

$$\frac{dV}{dt} \sim r(R) \times A(R) \quad (2)$$

If the $(PdCl_4)^{2-}$ precursor is sufficiently abundant that it does not limit the reaction rate and its concentration is uniform in the solution (which is fulfilled in our experiments; see Supporting Information (SI) section SI-1 and Figure S1), the observed growth of Pd in the initial regime (Figure 2a, i and ii) is controlled only by the concentration of the hydrated electrons, since the growth starts on uniformly sized Au seed particles; thus, the particles all have similar surface area, $A(R) =$ const. Hence, in this initial time regime the deposition rate of Pd^0 is limited by the concentration of the wet electrons that reduce the $(PdCl_4)^{2-}$ ions in the solution.[5] At longer times (Figure 2a, iii and iv), the particles closer to the excitation spot experience faster growth due to the higher concentration of e^-_{aq}. This causes systematic differences in particle size (i.e., capture area, A), which further accelerate the growth of particles near the excitation spot compared to more distant particles. In this regime, the dependence of both $r(R)$ and $A(R)$ is responsible for a significant spread of the particle volumes as a function of distance from the exciting beam.

Figure 2b shows an analysis of the time dependent particle volume due to Pd deposition on Au nanoparticles at different distances from the electron beam excitation. The particle volumes were determined from the projected area, measured in STEM images, assuming spherical particle shapes. We have carried out experiments comparing Pd growth on Au seed particles with growth on homogeneously nucleated Pd nanoparticles. The two situations show the same growth rates, showing that our conclusions are not affected by lattice mismatch etc. (see Supporting Information section SI-2 and Figure S3). After the first excitation cycle, the initially uniformly sized Au seed particles show significant Pd growth at a rate that

dx.doi.org/10.1021/ja508279v | J. Am. Chem. Soc. 2014, 136, 16865−16870

clearly depends on the distance R from the excitation spot. Overall, the particles closer to the beam experience faster growth due to the higher concentration of e^-_{aq} and the growth decreases with increasing R. At the initial stage (for time $t < 180$ s), it shows a relatively slow, linear increase in particle volume V with time (for particles more than 300 nm away from the beam). At a later stage (time $t > 180$ s), as expected, a significant acceleration and spread of the $V(R, t)$ at different distances is observed due to the increasing differences in the size of the nanoparticles.

Figure 2c shows the volume growth rate for these two distinct regimes, i.e., short and long times, determined from the measured $V(R, t)$. The plot clearly shows that the growth rate in both regimes depends on the distance from the exciting electron beam; significant growth occurs at distances as far as 1 μm away from the excitation, consistent with the long-range diffusion of the hydrated electrons generated by radiolysis at $R = 0$.

The reaction order of the redox reaction, $(PdCl_4)^{2-} + 2e^- \rightleftharpoons Pd^0 + 4Cl^-$, with respect to the concentration $[e^-_{aq}]$ of the hydrated electrons can be determined in two different ways: (i) from the dependence of the Pd growth rate on the distance R from the excitation spot, using the previously established result that $[e^-_{aq}](R) \sim R^{-1}$; and (ii) by comparing the Pd growth rates at the same distance R for different beam currents, assuming that $[e^-_{aq}]$ is proportional to the electron current for low dose rates. In the initial time regime in which the size of the Au seed particles is uniform and the Pd deposition rate depends only on $[e^-_{aq}]$, a power-law fit of the measured rate of Pd^0 production as a function of distance R gives an exponent (-1.1 ± 0.2). This implies that the rate of Pd^0 production is proportional to the concentration of hydrated electrons; that is, the redox reaction is a first order reaction with respect to the concentration of e^-_{aq}: $r = k[e^-_{aq}]^1 \cdot [(PdCl_4)^{2-}]^y$.

To confirm the reaction order, we performed a second set of experiments in which the electron beam current was increased by a factor of 2, while all other conditions were kept identical to the growth sequence shown in Figure 1 and analyzed in Figure 2. Measuring again the volume growth rate of Pd on Au seed particles as a function of the distance from the excitation spot, and comparing the rates of Pd^0 production for the two electron beam currents, we obtain the results shown in Figure 3. The red curve summarizes the Pd deposition rates at 400 pA beam current; the blue curve shows the rates resulting from a beam current of 200 pA. Both curves in Figure 3 show deposition rates in the initial time regime; the results for the growth induced by the 400 pA current at later stages are shown in Supporting Information section SI-1 and Figure S2. Doubling of the electron beam current results in an average increase of the volume growth rate by a factor of (2.2 ± 0.3), which confirms a first-order reaction with respect to the concentration of hydrated electrons, which reduce the tetrachloropalladate complexes to Pd^0. This also confirms that a linear regime is maintained at both beam currents used here, in which the concentration of hydrated electrons created by radiolysis is proportional to the current of the stationary, focused electron beam. Through diffusion of the hydrated electrons, an equilibrium concentration profile, $[e^-_{aq}](R)$, appears to be established essentially instantaneously on the time scale of our experiments. Hence, we find rates of Pd^0 production that are proportional to the beam current for nearly all distances R from the excitation. Only at very small distances from the exciting beam is the increase in Pd deposition rate between the two beam currents higher. This can be explained by the rapid increase in particle size at close separation, which causes a departure from the initial growth regime in which the rate of Pd deposition depends only on the concentration of the hydrated electrons.

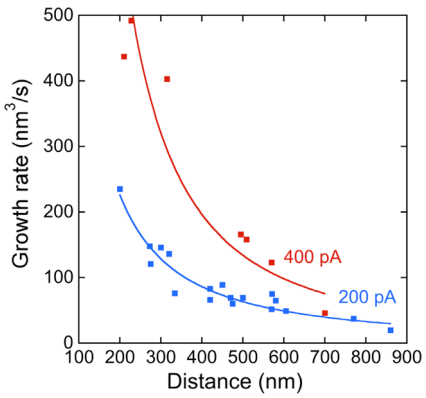

Figure 3. Comparison of the experimentally determined (Figure 2b) volume growth rate at two different electron beam currents: 200 pA (blue squares) and 400 pA (red squares) in the initial time regime between 0 and 180 s. The mean ratio of the growth rates for the two different electron currents is (2.2 ± 0.3).

3. COMPARISON WITH Au NANOPARTICLE SOLUTION GROWTH

Our results on the reduction of $(PdCl_4)^{2-}$ to Pd^0 by hydrated electrons produced by electron beam induced radiolysis in aqueous solution suggest that the deposition rate of zerovalent metal species on nanoparticles suspended in the solution provides a quant itative measurement of redox reaction rates in solution. To further confirm this conclusion, we have performed control experiments involving metal-ion complexes with different valence. The reduction of tetrachloropalladate to Pd^0 requires 2 electrons per $(PdCl_4)^{2-}$ ion. Aqueous solutions of $NaAuCl_4$ salt involve tetrachloroaurate $(AuCl_4)^-$ anions. Overall, the reduction of this Au chloro-complex to Au^0 requires the capture of 3 electrons per anion: $(AuCl_4)^- + 3e^- \rightleftharpoons Pd + 4Cl^-$. Gamma-radiolysis studies have shown that the reduction of the trivalent gold ions $(Au^{III}Cl_4)^-$ to metallic gold clusters proceeds in a stepwise fashion. The first step involves the reduction to $(Au^{II}Cl_4)^{2-}$ by capture of one hydrated electron,[23] followed by the disproportionation of Au^{II}:

$$2(Au^{II}Cl_4)^{2-} \rightarrow (Au^{III}Cl_4)^- + (Au^{I}Cl_2)^{2-} + 2Cl^-$$

At higher electron doses, the Au^{III} ions become partly depleted and the accumulating aurous (Au^I) ions compete for the available hydrated electrons, becoming reduced to zerovalent Au^0 atoms that are the precursors of Au clusters and nanoparticles. Similar to the radiolysis experiments, the irradiation of $NaAuCl_4$ aqueous solution in the liquid cell by the electron beam leads to the formation of gold nanoparticles. Figure 4a shows an initially homogeneous and uniform 10 μM $NaAuCl_4$ aqueous solution in the liquid cell. Local excitation by a stationary electron beam positioned at the points marked in Figure 4b–f results in homogeneous nucleation and growth of Au nanoparticles with brighter contrast. Even though we are not using suspended seed particles, as in the case of Pd growth, the size of the Au particles allows us to track the local

dx.doi.org/10.1021/ja508279v | J. Am. Chem. Soc. 2014, 136, 16865–16870

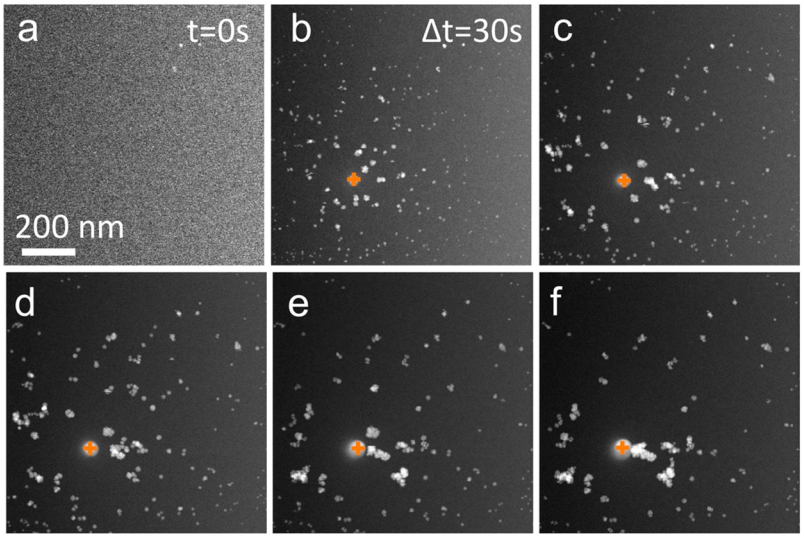

Figure 4. Electron beam effect on Au nanoparticle growth. (a–c) Au growth, induced by cycles of local focused electron beam exposure (30 s exposure; beam current: 300 pA; probe size: 0.2 nm) at the position marked by an orange cross. (a) Au precursor containing aqueous solution; (b) after 1 exposure; (c–f) after consecutive 30 s exposures. The bright feature at the position of the stationary beam spot (+) stems from local changes to the liquid cell membrane.

production of Au^0 via reduction of $(AuCl_4)^-$ by beam-induced hydrated electrons. The nucleation and growth behavior observed in Figure 4a–f is consistent with our conclusions for Pd. Local electron irradiation causes the production of e^-_{aq}, which spread by diffusion in the aqueous solution and in turn caused the reduction of a metal chloro-complex $(AuCl_4)^-$ to Au^0. The resulting supersaturation of Au^0 causes Au nanoparticle nucleation and growth in the solution. Images, taken after the image sequence in Figure 4, show that nucleation and growth of Au particles are observed as far as $R \sim 1.25$ μm away from the excitation spot, indicating that the hydrated electrons diffuse and, as a consequence, reduce the precursor and cause nucleation of nanoparticles—even further than the ~500 nm observed for Pd growth.[5] Remote areas of the solution remain unaffected, i.e., uniform without any formation of Au nanoparticles.

Figure 4 shows that even a brief (30 s) local exposure of the solution to the focused electron beam (beam current: 300 pA) results in the nucleation of Au nanoparticles; further exposures progressively increase their size. The single crystalline particles move readily in the solution, which gives rise to the pronounced clustering of Au particles observed at later stages in the image sequence. As for Pd growth, the size increase of the particles and the growth rate depend on the distance from the excitation spot, consistent with the focused beam of high-energy electrons producing radicals and a high local concentration of hydrated electrons (e^-_{aq}), which then disperse by diffusion.

An analysis of the image sequence of Figure 4 yields the dependence of the Au growth rate (i.e., rate of Au^0 production) on the distance from the excitation, as shown in Figure 5 for the initial stages of the growth. Given that the concentration of $NaAuCl_4$ (10 μM) is identical to the concentration of $PdCl_2$ in our Pd solution growth experiments, we can directly compare the rates at which zerovalent metal is produced in aqueous solutions of the two different salts.

We find a ratio of the Pd (200 pA beam current) to Au (300 pA) volume growth rates of ~1.25. Since the concentration of the metal precursor is the same, the rate at which zerovalent

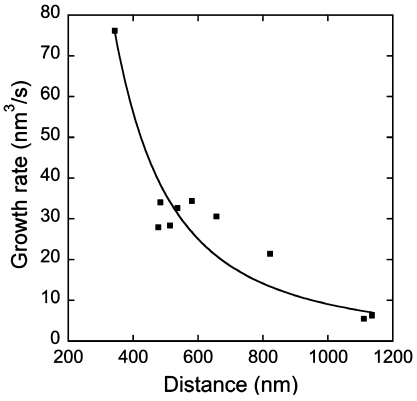

Figure 5. Experimentally determined, from the sequence in Figure 4; dependence of the particle volume growth rates as a function of distance from the excitation for 300 pA electron beam current in the initial time regime.

metal atoms are produced should only depend on the concentration of hydrated electrons (proportional to the beam current) and the valence of the anion complexes in the solution. Au nanoparticles nucleate and grow via reduction of tetrachloroaurate $[(AuCl_4)^-]$, in which the oxidation state of gold is Au^{3+}. The reduction to metallic Au^0 requires the capture of 3 electrons, while the reduction of tetrachloropalladate $[(PdCl_4)^{2-}]$ to Pd^0 is a 2-electron process. For the same concentration $[e^-_{aq}]$ of hydrated electrons, the ratio of Au^0:Pd^0 production rates should be $^2/_3$. In our case, different beam currents were used for the Pd and Au solution growth experiments; hence, the expected ratio is $1.5 \times 0.67 \sim 1.0$. The experimentally determined ratio is somewhat higher ($r(Pd^0)$:$r(Au^0)$ ~ 1.25); that is, the growth of Au is slightly slower than predicted. Possible origins of this minor deviation from the expected ratio of reaction rates are the need for initial nucleation of Au particles, in contrast to the deposition of Pd on preexisting Au seeds, and the uncertainties due to the facile motion and redistribution of Au particles in the solution.

dx.doi.org/10.1021/ja508279v | J. Am. Chem. Soc. 2014, 136, 16865–16870

4. CONCLUSIONS

In summary, we use the reduction of $(PdCl_4)^{2-}$ and $(AuCl_4)^-$ to Pd^0 and Au^0, respectively, by hydrated electrons produced by electron beam induced radiolysis in aqueous solution to demonstrate that in situ liquid cell TEM/STEM experiments can be used to reproducibly measure the rate of reduction of metal precursors in redox reactions. This can provide insight into the reaction mechanism, as demonstrated by determining the reaction order with respect to the concentration of hydrated electrons, the primary reducing agent in our experiments. Our results show that the deposition rate of zerovalent metal species on nanoparticles suspended in the solution provides a quantitative measurement of redox reaction rates in solution. By comparing redox reactions to Pd^0 and Au^0, which involve different numbers of transferred electrons per metal atom, we find that such indirect measurements of the reduction rate in solution are highly reproducible, due to the ability to precisely control both the concentration of the precursor salts and that of the electron beam-generated reactants. Our results thus pave the way for the broad use of liquid cell electron microscopy for the in situ, real-time monitoring of chemical reactions in solution.

5. MATERIALS AND METHODS

Solutions of palladium chloride ($PdCl_2$, Fisher Scientific) were made by dissolving 88.65 mg of the salt in 300 μL of HCl, which was then diluted with water to a concentration between 0.01 mM and 0.1 mM. For seeded growth, Au nanoparticles (British Biocell International) with 12 nm size and density 1.4×10^{12} particles/mL, were introduced in the solutions. Observations of Pd growth in the liquid cell were carried out at $PdCl_2$ concentrations of 10 μM $PdCl_2$ in the presence of 12 nm Au nanoparticles. Au nanoparticles growth was observed in 10 μM $NaAuCl_4$ aqueous solutions. The liquid experiments were carried out in a Hummingbird Scientific holder with liquid cells consisting of two 30 nm thick SiN membrane windows with 50 × 50 μm window area. The spacing between the windows was controlled using 250 nm SiO_2 spacer layers. STEM imaging was performed in a FEI Titan 80–300 environmental Cs-corrected (for TEM mode) microscope operated at 300 kV. The experiments were performed with electron beam: ~2 Å beam size and 200–400 pA current positioned for time intervals indicated on the images in Figures 1 and 4. The beam current was measured in vacuum before introduction of the liquid cell. The fluid path length is typically ~200–300 nm. The local fluid thickness determination is shown in Figure S4. The STEM images of the growth sequences were recorded with 1024 × 1024 pixels, 4 μs dwell time/pixel, 4.2 s/frame.

■ ASSOCIATED CONTENT

Supporting Information

Analysis of the equilibration of the precursor concentration via diffusion in the solution; comparison of Pd growth rate on Au and Pd nanoparticles; liquid thickness in the in situ liquid cell; supporting movies. This material is available free of charge via the Internet at http://pubs.acs.org.

■ AUTHOR INFORMATION

Corresponding Author

esutter@bnl.gov.

Notes

The authors declare no competing financial interest.

■ ACKNOWLEDGMENTS

This research has been carried out at the Center for Functional Nanomaterials, Brookhaven National Laboratory, which is supported by the U.S. Department of Energy, Office of Basic Energy Sciences, under Contract No. DE-AC02-98CH10886.

■ REFERENCES

(1) Zheng, H. M.; Smith, R. K.; Jun, Y. W.; Kisielowski, C.; Dahmen, U.; Alivisatos, A. P. *Science* **2009**, *324*, 1309.
(2) Parent, L. R.; Robinson, D. B.; Woehl, T. J.; Ristenpart, W. D.; Evans, J. E.; Browning, N. D.; Arslan, I. *ACS Nano* **2012**, *6*, 3589.
(3) Evans, J. E.; Jungjohann, K. L.; Browning, N. D.; Arslan, I. *Nano Lett.* **2011**, *11*, 2809.
(4) Liao, H. G.; Cui, L. K.; Whitelam, S.; Zheng, H. M. *Science* **2012**, *336*, 1011.
(5) Jungjohann, K. L.; Bliznakov, S.; Sutter, P. W.; Stach, E. A.; Sutter, E. A. *Nano Lett.* **2013**, *13*, 2964.
(6) Sutter, E.; Jungjohann, K.; Bliznakov, S.; Courty, A.; Maisonhaute, E.; Tenney, S.; Sutter, P. *Nat. Commun.* **2014**, *5*, 4946.
(7) Park, J.; Zheng, H. M.; Lee, W. C.; Geissler, P. L.; Rabani, E.; Alivisatos, A. P. *ACS Nano* **2012**, *6*, 2078.
(8) Williamson, M. J.; Tromp, R. M.; Vereecken, P. M.; Hull, R.; Ross, F. M. *Nat. Mater.* **2003**, *2*, 532.
(9) Gu, M.; Parent, L. R.; Mehdi, B. L.; Unocic, R. R.; McDowell, M. T.; Sacci, R. L.; Xu, W.; Connell, J. G.; Xu, P. H.; Abellan, P.; Chen, X. L.; Zhang, Y. H.; Perea, D. E.; Evans, J. E.; Lauhon, L. J.; Zhang, J. G.; Liu, J.; Browning, N. D.; Cui, Y.; Arslan, I.; Wang, C. M. *Nano Lett.* **2013**, *13*, 6106.
(10) de Jonge, N.; Peckys, D. B.; Kremers, G. J.; Piston, D. W. *P Natl. Acad. Sci. USA* **2009**, *106*, 2159.
(11) de Jonge, N.; Dukes, M. J.; Kremers, G. J.; Northan, B. M.; Peckys, D. B.; Ring, E. A.; Piston, D. W.; Sougrat, R. *Microsci. Microanal.* **2009**, *15*, 686.
(12) Mirsaidov, U. M.; Zheng, H. M.; Casana, Y.; Matsudaira, P. *Biophys. J.* **2012**, *102*, L15.
(13) Evans, J. E.; Jungjohann, K. L.; Wong, P. C. K.; Chiu, P. L.; Dutrow, G. H.; Arslan, I.; Browning, N. D. *Micron* **2012**, *43*, 1085.
(14) Mirsaidov, U. M.; Zheng, H. M.; Casana, Y.; Matsudaira, P. *Biophys. J.* **2012**, *103*, 165.
(15) Zheng, H. M.; Claridge, S. A.; Minor, A. M.; Alivisatos, A. P.; Dahmen, U. *Nano Lett.* **2009**, *9*, 2460.
(16) White, E. R.; Mecklenburg, M.; Shevitski, B.; Singer, S. B.; Regan, B. C. *Langmuir* **2012**, *28*, 3695.
(17) Zheng, H. M.; Mirsaidov, U. M.; Wang, L. W.; Matsudaira, P. *Nano Lett.* **2012**, *12*, 5644.
(18) Leong, F. Y.; Mirsaidov, U. M.; Matsudaira, P.; Mahadevan, L. *Phys. Fluids* **2014**, *26*, No. 012003.
(19) Lu, J.; Aabdin, Z.; Loh, N. D.; Bhattacharya, D.; Mirsaidov, U. M. *Nano Lett.* **2014**, *14*, 2111.
(20) Kraus, T.; de Jonge, N. *Langmuir* **2013**, *29*, 8427.
(21) Grogan, J. M.; Schneider, N. M.; Ross, F. M.; Bau, H. H. *Nano Lett.* **2014**, *14*, 359.
(22) Boag, J. W.; Hart, E. J. *Nature* **1963**, *197*, 45.
(23) Dey, G. R.; El Omar, A. K.; Jacob, J. A.; Mostafavi, M.; Belloni, J. *J. Phys. Chem. A* **2010**, *115*, 383.